Journal of
Applied Crystallography
ISSN 0021-8898

Two-dimensional intensity profiles of effective satellites

S. L. Morelhão, L. H. Avanci, A. A. Quivy and E. Abramof

Journal of
Applied
Crystallography
ISSN 0021-8898

Received 20 September 2001
Accepted 7 November 2001

Two-dimensional intensity profiles of effective satellites

S. L. Morelhão,[a]* L. H. Avanci,[a] A. A. Quivy[b] and E. Abramof[c]

[a]Instituto de Física, USP, FAP, CP 66318, 05315-970 São Paulo, SP, Brazil, [b]Instituto de Física, USP, LNMS, CP 66318, 05315-970 São Paulo, SP, Brazil, and [c]Instituto Nacional de Pesquisas Espaciais, LAS, CP 515, 12201-970 São José dos Campos, SP, Brazil. Correspondence e-mail: morelhao@if.usp.br

The observation of a new X-ray scattering process with synchrotron radiation is reported. The phenomenon is analogous to three-beam diffraction in a single crystal; however, the features in the azimuthal scans are provided by superlattice-satellite reflections instead of bulk reflections. These features were named effective satellites and they are observed over the ordinary satellite reflections as a function of the azimuthal angle. Their occurrences have been monitored in completely different superlattices by mapping the incidence and azimuthal angles of the incident X-ray beam. Effects of structural parameters of the superlattices on the effective satellites as well as the information that can be extracted by measuring their positions are discussed.

1. Introduction

In the research and development of semiconductor devices for micro- and optoelectronic applications, X-ray diffraction is a very important non-destructive characterization tool. Double-crystal rocking curves and reciprocal-space mapping are standard and powerful high-resolution diffraction techniques for analyzing semiconductor epitaxic structures. These techniques investigate the X-ray scattering by the sample on a two-beam diffraction geometry, which implies that all features relevant to diffraction physics are described in the plane of incidence, *i.e.* the plane defined by the incident and diffracted beams. Consequently, in the commercially available ready-to-use diffractometers for high-resolution diffraction, the X-ray beam is mostly conditioned in the plane of incidence.

Recently, in searching for alternative methods of semiconductor analysis on high-resolution diffractometers, the reciprocal space around a Bragg surface diffraction (BSD) was investigated (Morelhão & Abramof, 1999). The BSD is a particular three-beam diffraction where an extreme asymmetric secondary reflection (grazing diffracted beam) is excited along with a primary symmetric Bragg reflection. More details on the BSD geometry are given below (see also Campos *et al.*, 1998; Avanci & Morelhão, 2000). The reciprocal-space analysis of the BSD has shown experimentally that its wavefield has a stronger attenuation in depth than that of the same Bragg reflection alone. In order to check if this property of the BSD would be useful for studying substrate surface damage due to epitaxic growth, the reciprocal-space analysis was also carried out on the BSD of heteroepitaxial superlattice structures. This led to some results that suggest the occurrence of effective satellites, as also reported by Morelhão & Abramof (1999). Since in standard high-resolution X-ray diffractometers the incident beam is not conditioned perpendicularly to the plane of incidence (the beam divergence is about 1° in this direction), the investigation of effective satellites is hindered by this type of equipment.

In this article, we further investigate the excitation condition of the BSD in semiconductor substrates as well as in different types of superlattices. We have accomplished two-dimensional mapping of the BSD by combining rocking curves (ω scans) with azimuthal scans. A synchrotron X-ray beam, also conditioned in the direction perpendicular to the plane of incidence, is used to improve the signal of the effective satellites and the resolution of the azimuthal scans. Discussions on the relevance of effective satellites to the study of superlattices are also presented.

2. Basic theory

Three-beam diffraction arises when an incident monochromatic beam simultaneously satisfies the Bragg law for two reflections within a crystal. In most case, it is generated when the crystal is first aligned by an ω rotation (the rocking angle) for a symmetric Bragg reflection, the primary reflection **P**. The φ rotation (the azimuthal angle) of the crystal around the diffraction vector of the primary reflection, **P**, causes another reflection, the secondary reflection **S**, to diffract simultaneously. The primary and secondary beam directions are given by the wavevectors $\mathbf{k}_P = \mathbf{P} + \mathbf{k}_0$ and $\mathbf{k}_S = \mathbf{S} + \mathbf{k}_0$, respectively, where $\mathbf{k}_0$ is the wavevector of the incident beam. Although, there is symmetry in the energy balance from one beam to another, we will concern ourselves here only with the extra amount of intensity transferred from the secondary beam to the primary beam. The coupling reflection C is responsible for such a transfer since $\mathbf{k}_P = \mathbf{C} + \mathbf{k}_S$. In terms of the incident beam direction, it can be expressed as $\mathbf{k}_P = \mathbf{C} + \mathbf{S} + \mathbf{k}_0$, or $\mathbf{k}_P = \mathbf{P}^* +$

$\mathbf{k}_0$, where $\mathbf{P}^* = \mathbf{C} + \mathbf{S}$ is the reciprocal vector of the effective primary reflection, also known as the detour reflection. Hereinafter, the asterisk * is used to specify *effective* diffraction peaks.

The BSD is a type of three-beam diffraction, frequently encountered in multiple-diffraction experiments, where $|\mathbf{S}| = |\mathbf{C}|$ and $\mathbf{S} \cdot \mathbf{P} = |\mathbf{P}|^2/2$, and consequently, the secondary beam, $\mathbf{k}_S$, is scattered at a shallow angle with the surface (it may even be in the surface-parallel direction for perfectly on-cut crystal surfaces). The excitation of the effective primary reflection, $\mathbf{P}^*$, depends on the azimuthal position of the crystal, since the secondary reflection must be excited. By monitoring a weak primary reflection, the occurrence of the effective reflection is clearly observed in the azimuthal scan. However, when probed with an intense and collimated incident beam as a function of the ω and φ angles, the profile of the BSD peak is composed of contributions from different diffraction cones. To illustrate this point, we present in Fig. 1 the ω:φ map of a BSD for a total forbidden primary reflection, namely the 002 Si reflection. Besides the streak of the Bragg cone for the primary reflection (the horizontal streak), which is visible in this case exclusively due to the effective reflection, the long diagonal streak marks the positions where the secondary reflection is excited, *i.e.* the Bragg cone for the secondary reflection. The exact BSD angular condition is given at the intersection of the cones. Assuming an on-cut surface, above the primary streak ($\Delta\omega > 0$) the secondary beam is transmitted, and below ($\Delta\omega < 0$) it is reflected.

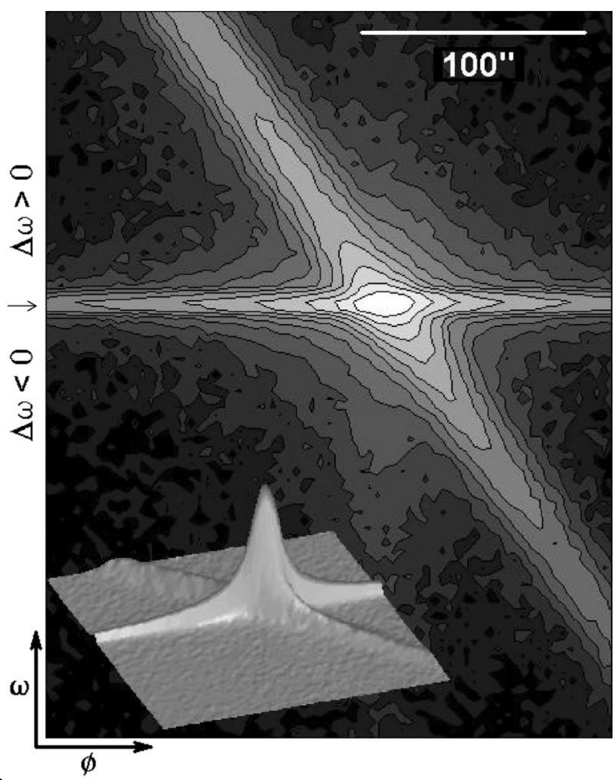

Figure 1
High-resolution ω:φ mapping of the $002^* = \bar{1}11 + 1\bar{1}1$ Bragg surface diffraction of a high-quality [001]-oriented Si crystal. The horizontal and diagonal streaks give the positions of the 002 and $\bar{1}11$ Bragg cones, respectively. The secondary beam is transmitted (reflected) for $\Delta\omega > 0$ ($\Delta\omega < 0$). Experimental conditions (only for this result): wiggler beamline (station 16.3, Daresbury, UK), four-bounce 111 Si monochromator, X-ray photon energy of 8339.3 eV (λ = 1.48676 Å), step width of 3.6 arcsec (both axes), divergence less than 5 arcsec (both axes). The maximum peak intensity is 426952 counts s^{-1}. The contour map and the three-dimensional surface (inset) show the log- and root-square-transformed intensities, respectively. This map is shown here for illustrative purposes only.

Superlattices are heteroepitaxial structures grown on top of single-crystal substrates and made of a repetition of an identical sub-structure of epilayers (the base epilayers). Their large periodicity, D, in real space gives rise to several satellite reflections that are visible due to the X-ray scattering by the reflections of the crystalline lattice in the epilayers of the base. With respect to the substrate reciprocal vectors, $\mathbf{G}$, the satellites are located in the reciprocal space by vectors such as $\mathbf{G}^{(n)} = \mathbf{G} + (\Delta q_G + n/D)\hat{z}$, where $\hat{z}$ is the surface-normal direction, n is the satellite index, 0, ±1, ±2 . . . , and $\Delta q_{\rm G}$ is the distance of the zeroth-order satellite (SL0, $n = 0$) from $\mathbf{G} \cdot \hat{z}$, the normal component of $\mathbf{G}$.

3. Theory of effective satellites

Besides the expected $\mathbf{P}^{(n)} = \mathbf{P} + (\Delta q_P + n/D)\hat{z}$ satellite reflections around the substrate primary reflection, $\mathbf{P}$, the effective satellites would be extra features that also depend on the azimuthal sample position, and they are visible near the substrate effective reflections, $\mathbf{P}^* = \mathbf{S} + \mathbf{C}$. However, instead of normal secondary and coupling reflections from a crystalline lattice, the effective satellites would have these reflections given by the satellite reflections $\mathbf{S}^{(s)} = \mathbf{S} + (\Delta q_S + s/D)\hat{z}$ and $\mathbf{C}^{(c)} = \mathbf{C} + (\Delta q_C + c/D)\hat{z}$, respectively. Therefore,

$$\mathbf{P}^{*(s+c)} = \mathbf{S}^{(s)} + \mathbf{C}^{(c)} = \mathbf{P} + [\Delta q_S + \Delta q_C + (s+c)/D]\hat{z} \qquad (1)$$

are the diffraction vectors of the effective satellites, and their excitement condition requires that both vectors, $\mathbf{P}^{*(s+c)}$ and $\mathbf{S}^{(s)}$, diffract simultaneously the incident beam. In other words, both vectors must be touching the surface of the Ewald sphere at the same time in order to excite an effective satellite. This will assure that the $\mathbf{C}^{(c)}$ reflections (the satellite coupling reflections) are under the diffraction condition to couple the beam scattered by the $\mathbf{S}^{(s)}$ reflections (the satellite secondary reflections).

The ω and φ angles for exciting an effective satellite are easily determined by assuming that the surface-normal direction is aligned with the substrate primary reflection. With such a simplification, the ω incidence angle for the effective satellites will be given by

$$\sin\omega = \lambda|P^{*(s+c)}|/2, \qquad (2)$$

and the φ angle by (Cole *et al.*, 1962)

$$\cos(\varphi - \alpha) = [\lambda|\mathbf{S}^{(s)}|/2 - \sin\omega\cos\gamma]/\cos\omega\sin\gamma, \qquad (3)$$

where γ and α are the polar and azimuthal angles describing the $\mathbf{S}^{(s)}$ vectors in the $\hat{x}$, $\hat{y}$ and $\hat{z}$ orthogonal system of unit vectors. $\hat{x}$ and $\hat{y}$ define the surface plane.

It should be noted that there are several $\mathbf{P}^{*(s+c)}$ effective satellites with the same ω angle of the $\mathbf{P}^{(n)}$ satellite, where $n = s$

Table 1
Parameters of the investigated superlattice structures obtained from high-resolution X-ray diffraction analysis.

D is the SL period, n_a/n_b are the number of monolayers in the a and b layers of the $[a/b]$ base layer, Δq_{002} is the longitudinal distance to the zeroth-order satellite from the 002 substrate reciprocal-lattice point, and $\langle a \rangle$ is the average lattice parameter of the SL.

	10×[Si/Ge]/Si(001)	10×[GaAs/AlAs]/GaAs(001)
D (Å)	296.41 (2)	1223 (10)
n_a/n_b	213/5	395/469
Δq_{002} ($\times 10^{-3}$ Å^{-1})	−0.5283 (31)	−0.545 (12)
$\langle a \rangle$ (Å)	5.438703 (44)	5.6621 (2)

+ c. Or, in other words, the SLn^* may be formed by contributions from a set of different $\mathbf{S}^{(s)} + \mathbf{C}^{(c)}$ detour paths, those that have the sum $s + c$ equal to the effective satellite index, n. For simplicity, each possible detour path for a given effective index will be denoted hereinafter by (s, c). However, even with the constraint of a common effective index, the (s, c) paths do not occur exactly at the same azimuthal angle. Their φ positions depend explicitly on the s index, as given by equation (3). Moreover, these paths also differ from one to another by the δ angle in which the satellite secondary beam [the beam diffracted by the $\mathbf{S}^{(s)}$ satellite secondary reflection] crosses the interfaces of the layers. δ can be calculated by

$$\cos(\pi/2 - \delta) = \lambda \mathbf{k}_S^{(s)} \cdot \hat{z}, \tag{4}$$

where $\mathbf{k}_S^{(s)} = \mathbf{S}(s) + \mathbf{k}_0$ and the direction of the $\mathbf{k}_0$ vector is defined by the ω and φ values obtained from equations (2) and (3). For a chosen BSD, the satellite secondary beam direction is parallel to the interfaces, $\delta = 0$, in all detour path where $s = c$.

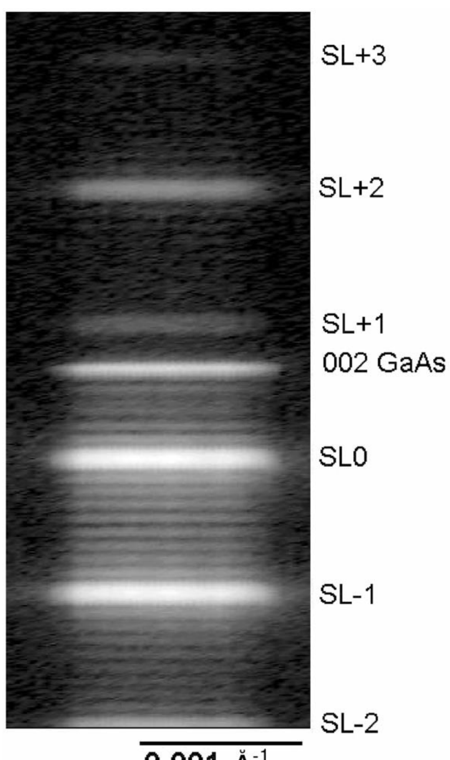

Figure 2
Reciprocal-space mapping of the 002 reflection in the GaAs/AlAs superlattice. The relative maximum intensities of the rods, from SL−2 to SL+2, are 7.6, 84.2, 100 (4291 counts s^{-1}), 27.1, 0.7 and 2.6%. The accentuated lateral broadening of the substrate and satellite rods indicates the presence of a high level of in-plane defects in the 1 μm GaAs buffer layer as well as in the superlattice structure. The map shows the log-transformed intensity. Measurements were carried out using a high-resolution X-ray diffractometer.

4. Experimental

The experiments were carried out at the X-ray diffraction beamline of the National Synchrotron Light Source/LNLS, Brazil. The beamline four-crystal monochromator (Tolentino & Rodrigues, 1992) was set to deliver X-ray photons with a wavelength λ of 1.43995 (12) Å. It was checked by a procedure similar to that applied elsewhere (Morelhão *et. al.*, 1998). The horizontal beam divergence was limited by slits, and its value of 18 arcsec was estimated by rocking curves of the 111 Si reflection; the vertical beam divergence of 9 arcsec was determined similarly. Rocking curves with horizontal or vertical planes of incidence, *i.e.* with π, σ, or any other linear polarization state, are possible at the LNLS with the three-axis goniometer (ω, φ and 2θ). In this goniometer, the ω and φ axes were built perpendicular to each other, and both have a minimum step size of 0.0004°. The orthogonal arcs of the motorized goniometric head carry out the alignment of a diffraction vector to the φ axis. Moreover, the goniometer was mounted on top of a χ table, which is able to rotate the plane of incidence of the goniometer from $\chi = -90$ to 90°. At $\chi = 0$ the plane of incidence is horizontal and at $\chi = \pm 90°$ it is vertical (the plus and minus signs indicate that the detector is above and below the horizontal plane of the storage ring, respectively). The intensities have been measured by a fast scintillation detector (the EDRa detector from Bede Scientific Instruments Ltd) with a maximum counting rate of 1.3 Mhz and high linearity, up to at least 400000 counts s^{-1}. The result in Fig. 1 was obtained with the same detector, although another experimental setup was used, as explained in the figure caption.

Two superlattices, 10×[Si/Ge]/Si(001) and 10×[GaAs/AlAs]/GaAs(001), were used here to investigate experimentally the existence of effective satellites. The samples were first characterized with Cu $K\alpha_1$ in the high-resolution X-ray diffractometer, at INPE, and their parameters obtained from rocking-curve analysis by dynamical simulation. The parameters are given in Table 1; the experimental setup of the diffractometer is described elsewhere (Morelhão & Abramof, 1999). The reciprocal-space mapping of the GaAs/AlAs superlattice in Fig. 2 was also performed using this diffractometer. A substrate miscut has been found only in the first sample, the Si/Ge superlattice. It is 0.6 (1)° towards the $[1\bar{1}0]$ directions, as measured on the three-axis goniometer at LNLS after aligning the [001] direction with the φ axis. In both samples, the in-plane [110] direction was taken as reference for the φ rotation ($\varphi = 0$).

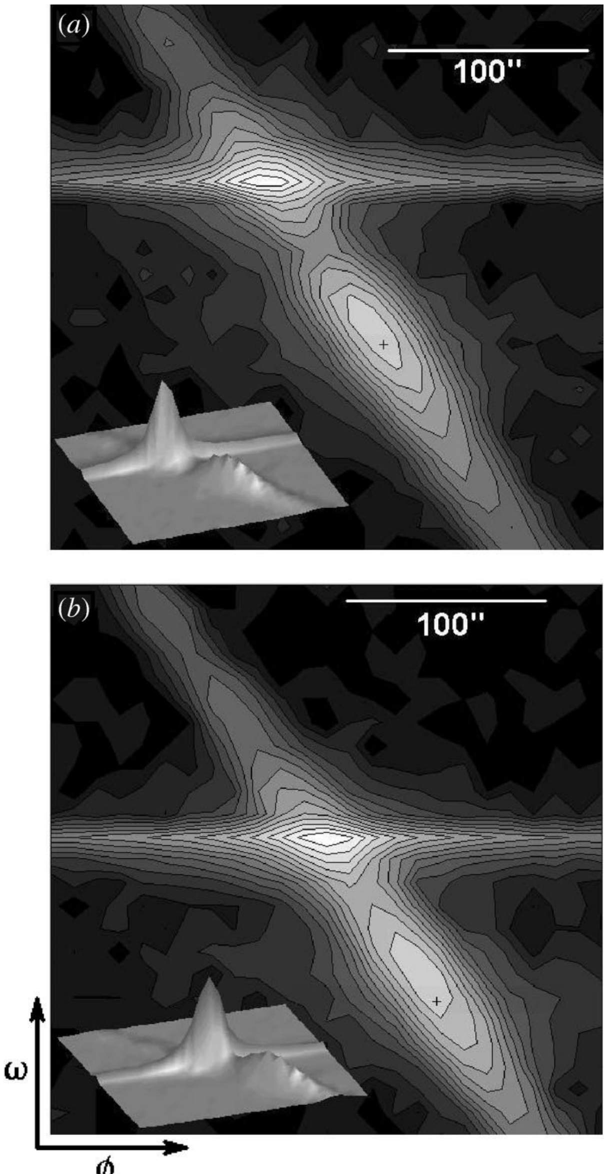

Figure 3
Two-dimensional ω:φ mapping around the (*a*) 002* = $\bar{1}11 + 1\bar{1}1$ and (*b*) 002* = $\bar{1}\bar{1}1$ + 111 substrate Bragg surface diffractions in the Si/Ge superlattice. Besides the substrate reflections, the maps also show the SL0* effective satellites, the expected positions of which, according to the values in Table 1, are given by the + marks. The contour maps and the three-dimensional surfaces (insets) show the log- and root-square-transformed intensities, respectively. The maximum intensities are 111536 (*a*) and 172068 counts s^{-1} (*b*). Mesh resolution: 0.0032° (step size in the ω and φ axes).

5. Results and discussion

According to the notation **P*** = **S** + **C**, the substrate BSDs chosen for our measurement have the 002* primary reflection formed by 111 reflections such as $1\bar{1}1 + \bar{1}11$ = 002*. The ω:φ maps of these BSDs for both samples are shown in Figs. 3 and 5. The predicted positions of the effective satellites are marked in the maps [calculated by equations (2) and (3) using the superlattice parameters in Table 1]. Besides the primary and secondary streaks of the substrate (clearly seen in all maps), the weak SL0* is the only measurable effective satellite in the Si/Ge superlattice (Figs. 3*a* and 3*b*). On the other hand, the excitement of five effective satellites, SL0*, SL±1* and SL±2*, has been measured in the GaAs/AlAs superlattice (Fig. 5). They occur at the positions where the substrate secondary streak crosses the ω positions of the ordinary satellites of the superlattice. Although the excitement of the effective satellites coincides with the secondary streak, they are not physically related, *i.e.* the occurrence of effective satellites does not depend on the substrate secondary reflection. It is only a coincidence that is imposed by equation (3), which is much more sensitive to the variations in the ω angle and in the in-plane lattice parameters than in the $\hat{z}$ component of the $\mathbf{S}^{(s)}$ reciprocal vectors (Morelhão & Cardoso, 1993).

The two ω:φ maps for the Si/Ge superlattice structure shown in Fig. 3 were recorded in two orthogonal directions, φ = 5.579° (**S**: $\bar{1}11$ and **C**: $1\bar{1}1$) and φ = 95.579° (**S**: $\bar{1}\bar{1}1$ and **C**: 111), which are discriminated by the substrate miscut. In the angular range of these maps, the substrate secondary beam, $\mathbf{k}_S = \mathbf{S} + \mathbf{k}_0$, is scattered above ($\mathbf{k}_S \cdot \hat{z} > 0$) and below ($\mathbf{k}_S \cdot \hat{z} < 0$) the superlattice/substrate interface, respectively. The only difference between these two maps is the small shift of the SL0* position, which is also a consequence of the substrate miscut that has tilted $\mathbf{P}^{*(0)}$ towards the [$1\bar{1}1$] direction, as illustrated in Fig. 4. It demonstrates that the effective satellites occur even when the substrate secondary beam does not cross the interface towards the superlattice. Geometrically, $\mathbf{P}^{*(0)}$ could be formed by the detour path (0, 0) as well as by the (±1, ∓1) path; however, these two paths are not alike since their φ position would be about 10 arcsec off the measured one, and also because of the much lower reflectivity of the first-order

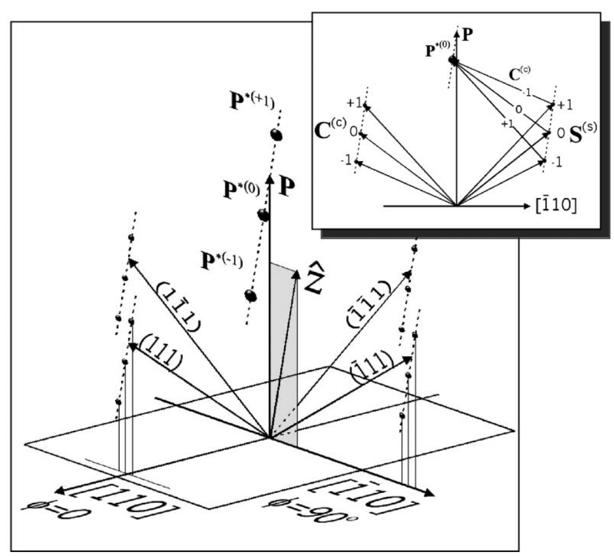

Figure 4
Reciprocal-space construction for the substrate secondary (or coupling) diffraction vectors, **S** (or **C**), and the primary one, **P**. The circles above and below the substrate vectors show the relative positions of the satellite reflections. The figure also illustrates the effect of a substrate miscut toward the [$\bar{1}10$] direction on the position of the satellites, $\mathbf{P}^{*(s+c)}$, $\mathbf{S}^{(s)}$ or $\mathbf{C}^{(c)}$. $\hat{z}$ is the surface-normal direction. The inset shows the formation of $\mathbf{P}^{*(0)}$ by three different detour paths, (0, 0) and (±1, ∓1), around the 002* = $\bar{1}11 + 1\bar{1}1$ substrate BSD.

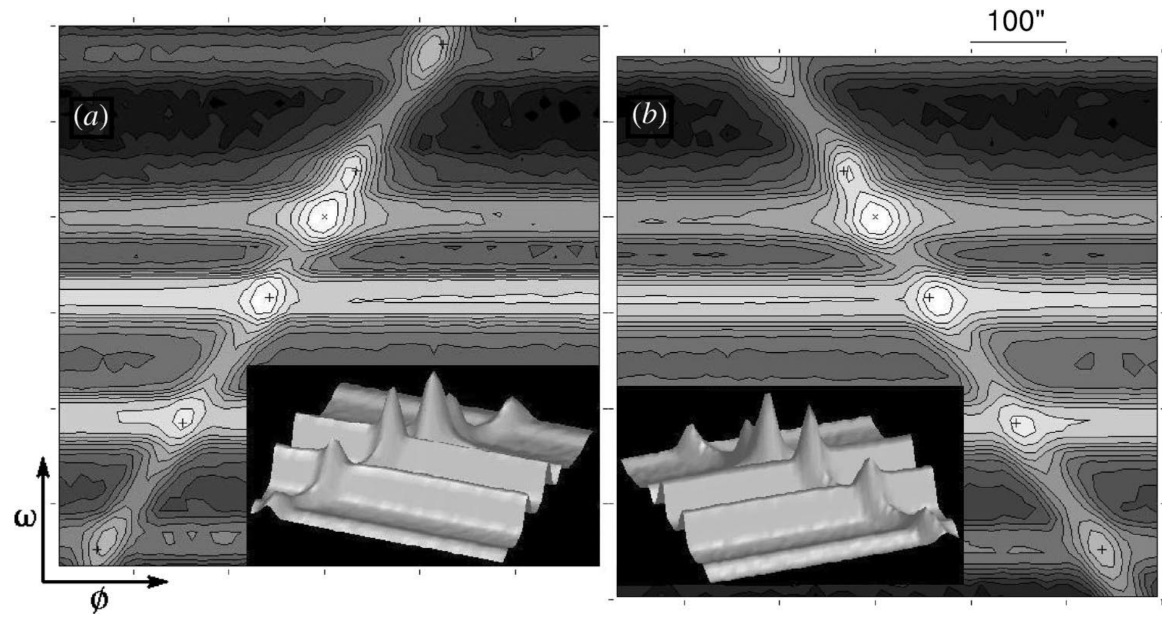

Figure 5
Two-dimensional ω:φ mapping around the (*a*) 002* = $\bar{1}11$ + $1\bar{1}1$ and (*b*) 002* = $1\bar{1}1$ + $\bar{1}11$ substrate Bragg surface diffractions in the GaAs/AlAs superlattice. Their (ω_0, φ_0) positions, marked with ×, are (14.7562°, −5.3434°) and (14.7562°, 5.3434°), respectively. Besides the substrate and superlattice ordinary reflections, the mapped intervals also shown five effective satellites, SL0*, SL±1*, and SL±2*, the theoretical positions of which [equations (2) and (3), and Table 1] are given by the + marks. The contour maps and the three-dimensional surfaces (insets) show the log- and root-square-transformed intensities, respectively. The maximum intensities are 106576 (*a*) and 97726 counts s^{-1} (*b*). Mesh resolution: 0.0032°.

satellites, as can be checked in the rod scan of the 004 reflection presented elsewhere (Fig. 5 of Morelhão & Abramof, 1999). Due to the short periodicity of the superlattice in real space, which increases the distance of the satellites in the reciprocal space, it is expected that the first-order satellites around the 111 reflections are also weak reflections.

Effective satellites formed by satellite secondary and coupling reflections of mixed index are seen in the ω:φ maps of the GaAs/AlAs superlattice, Fig. 5. All $\mathbf{P}^{*(n)} = \mathbf{S}^{(s)} + \mathbf{C}^{(c)}$ where the effective index, $n = s + c$, is an odd number must have $s \neq c$. Then, the SL±1* have their major intensity contributions from the following detour paths: (±1, 0), (0, ±1), (∓1, ±2) and (±2, ∓1). Each one of these paths has a slightly different φ position, less than 2 arcsec, which does not allow a discrimination of their individual contributions by scanning the azimuthal positions of the effective satellites, as shown in Fig. 6. Physically, these paths also differ from one another by the δ angle [the angle in which the secondary beam crosses the interfaces of the layers, as given by equation (4)]. For the first couple of detour paths, δ is just 125 arcsec. This value is smaller than the critical grazing angle for the X-ray beam to cross the AlAs/GaAs interfaces, 141 arcsec, the difference between the critical angles for these materials with the air. Therefore, the SL±1* may be exclusively formed by the (∓1, ±2) and (±2, ∓1) paths. Other paths with higher-order satellite reflections, where $s + c$ is also equal to ±1, are geometrically possible, but they should be too weak to be measurable. It can also be assumed that the SL0* should mainly be formed by the (0, 0) path, the SL+2* by the (0, +2) and (+2, 0) paths, and the SL−2* by the (−1, −1), (0, −2) and (−2, 0) paths.

There are some discrepancies between the measured and calculated (+ marks in Fig. 5) positions of the effective satellites, smaller than the angular resolution (0.0032°) used in the data acquisition, even though the average position of the reference direction calculated from the SLn* positions is at φ = 2.2 ± 2.8 arcsec. It confirms that there is no in-plane rotation of the superlattice with respect to the substrate lattice.

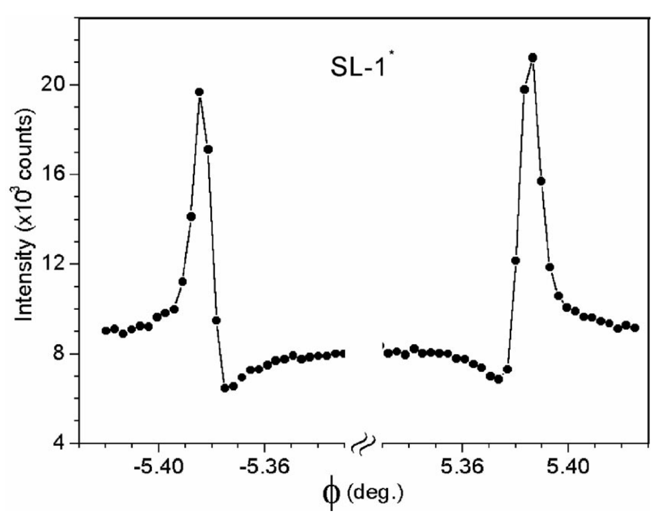

Figure 6
Detailed azimuthal profiles of the SL−1* effective satellites mapped in Fig. 5. The incidence angle correspond to the ω position of the SL−1 satellite, about −214 arcsec from the 002 GaAs reflection.

Moreover, within our resolution in the φ position, the effective satellite peaks fall exactly over the substrate secondary streak, indicating that the superlattice exhibits no relaxation. Otherwise, the imaginary line connecting the effective satellites would be shifted in φ from the secondary streak, or the φ position of the BSD, by $\Delta\varphi = -5.8 \times 10^4(\Delta a/a)_{\|}$ arcsec, where $(\Delta a/a)_{\|}$ is the in-plane lattice mismatch [the numeric value of this ratio was calculated from equation (3)]. For instance, in the scans $\Delta\varphi$ is not larger than 10 arcsec; then the shift in the parallel lattice parameter of the superlattice would be less than 0.001 Å.

The asymmetry in the profiles of the SL$-$1* shown in Fig. 6 demonstrates that the coherence of the wavefield scattered by the effective satellite is preserved through the detour path, and it is interfering with the wavefield from the satellite-primary reflection. Similar asymmetries are observed in the φ scan of n-beam diffraction in bulk crystals, where they are studied as a solution of the 'phase problem' (Chang, 1984; Weckert & Hümmer, 1997). In the case of superlattices, the phase angles (φ) of the satellite reflections are due to the wavefield scattered by the base layers at the positions of the satellites, which is not only defined by the structure factors of the reflections of the layers but also by their thickness. Mathematically, the wavefield of the base, normalized by the number of unit cells in the diffracting area of the sample, can be written as

$$\begin{aligned} D(\mathbf{G}) &= F_a(\mathbf{G}) \sum_{p=1}^{N_a} \exp[-2\pi i \mathbf{G} \cdot \hat{z}(pc_a)] \\ &\quad + F_b(\mathbf{G}) \sum_{p=N_a+1}^{N_a+N_b} \exp[-2\pi i \mathbf{G} \cdot \hat{z}(pc_b)] \\ &= |D(\mathbf{G})| \exp(i\varphi), \end{aligned}$$

where the subscripts a and b specify the two layers constituting the base, $F_{a,b}$ are the structure factors of the crystalline lattices, $N_{a,b}$ are the number of unit cells along the z direction, $c_{a,b}$ are the perpendicular lattice parameters, and $\mathbf{G}$ stands for $\mathbf{G}^{(n)}$, the reciprocal vector of the satellite reflections. Since the phases depend on the thickness of the layers, the occurrence of the asymmetries should be more sensitive to the perfect repetition of the layers than to the crystalline perfection of the individual layers, as in the case of this sample. The reciprocal-space map in Fig. 2 confirms that the sample has a good superlattice periodicity (high number of fringes between the SL reflections) and a poor lateral crystalline perfection, which is evident by the accentuated lateral broadening of the substrate and superlattice reflections.

Another feature to be noted in Fig. 5 is the absence of an interaction between the substrate and superlattice reflections. Such interaction would be hybrid paths with the substrate secondary beam coupled by satellite reflections or *vice versa*, the satellite secondary beam coupled by substrate reflections. In terms of their reciprocal vectors, the effective hybrid satellites would be given by

$$\mathbf{P}^{*(1/2+c)} = \mathbf{S} + \mathbf{C}^{(c)} = \mathbf{P} + [\Delta q_C + c/D]\hat{z}$$

and

$$\mathbf{P}^{*(s+1/2)} = \mathbf{S}^{(s)} + \mathbf{C} = \mathbf{P} + [\Delta q_S + s/D]\hat{z},$$

respectively. The half index stands for the fact that $\Delta q_S = \Delta q_C = \Delta q_P/2$ for any BSD. The $\mathbf{P}^{*(s+1/2)}$ satellites can only occur when the substrate secondary beam is a reflected beam, *i.e.* diffracted towards the superlattice. Therefore, the expected $\omega{:}\varphi$ position of this type of satellite would be over the secondary streak, half way between the superlattice satellites, and in the region of the map below the primary streak ($\Delta\omega < 0$). The absence of any extra feature at these positions, besides the secondary streak itself, indicates that at grazing angles, $\delta \simeq 150$ arcsec, the substrate secondary beam is not able to interact with the structure of $\mathbf{C}^{(c)}$ satellites coupling reflections. This value for the δ angle was estimated by equation (4), with $\mathbf{k}_S^{(s)}$ replaced by $\mathbf{k}_S$, and the $\mathbf{k}_0$ corresponding to the $\omega{:}\varphi$ position at the middle of the SL$-$1* and SL$-$2* satellites.

6. Conclusions

In summary, we have reported here the observation of effective satellites in different types of superlattice structures using synchrotron radiation. Such features are the extra intensity contribution over the ordinary superlattice satellite reflections and they depend on the azimuthal sample position. Although their angular conditions resemble the multiple-diffraction phenomenon in crystals, there is an intrinsic difference between the two scattering processes. Multiple diffraction occurs due to the three-dimensional nature of the crystalline lattices, while the effective satellites are produced by the one-dimensional periodicity of the superlattice plus the in-plane atomic periodicity of the epitaxic layers. Their occurrence can change the intensity ratios of the normal satellites in rocking-curve measurements, when carried out with an X-ray beam of low azimuthal divergence. They could jeopardize the characterization of superlattice structure in synchrotron facilities where small beam divergences are normally used. The φ positioning of the effective satellites around the reference direction would allow a direct measurement of the in-plane rotation of the superlattice with respect to the substrate lattice. Further exploration of the phenomenon may also provide information on the relaxation of the superlattice as well as on its structural perfection.

References

Avanci, L. H. & Morelhão, S. L. (2000). *Acta Cryst.* A**56**, 507–508.

Campos, C., Sanjurjo, N. L. & Chang, S. L. (1998). *Phys. Lett. A*, **246**, 441–445.

Chang, S. L. (1984). *Multiple Diffraction of X-rays in Crystals.* Heidelberg: Spring Verlag.

Cole, H., Chambers, F. W. & Dunn, H. M. (1962). *Acta Cryst.* **15**, 138–144.

Morelhão, S. L. & Abramof, E. (1999). *J. Appl. Cryst.* **32**, 871–877.

Morelhão, S. L. & Cardoso, L. P. (1993). *J. Appl. Phys.* **73**, 4218–4226.

Morelhão, S. L., Hayashi, M. A., Avanci, L. H., Cardoso, L. P. & Collins, S. P. (1998). *Appl. Phys. Lett.* **73**, 2194–2196.

Tolentino, H. & Rodrigues, A. R. D. (1992). *Rev. Sci. Instrum.* **63**, 946–949.

Weckert, E. & Hümmer, K. (1997). *Acta Cryst.* A**53**, 108–143.